Thermal and Chemical Expansion of Sr-Doped Lanthanum Cobalt Oxide ($La_{1-x}Sr_xCoO_{3-\delta}$)

Xiyong Chen,[†] Jinsong Yu,[‡] and Stuart B. Adler*,[†]

Department of Chemical Engineering, University of Washington, Box 351750, Seattle, Washington 98195-1750, and Department of Chemical Engineering, Case Western Reserve University, 10900 Euclid Avenue, Cleveland, Ohio 44106

Received April 28, 2005. Revised Manuscript Received June 1, 2005

The equilibrium thermal expansivity (β_T) and oxygen-vacancy chemical expansivity (β_C) of polycrystalline $La_{1-x}Sr_xCoO_{3-\delta}$ (LSC; $x = 0.2$, 0.4, and 0.7) have been measured at 600 °C $< T <$ 900 °C and 10^{-4} atm $< P_{O_2} <$ 0.21 atm using controlled-atmosphere dilatometry. These measurements show only a moderate dependence of β_T on temperature, suggesting that increases often observed in the coefficient of thermal expansion when measured at constant P_{O_2} are primarily thermally induced chemical expansion associated with changes in oxygen stoichiometry. The dependences of β_T and β_C on the temperature, oxygen-vacancy concentration, and Sr content (x) were characterized and found to follow a consistent nonlinear trend, which may result from the relaxation of lattice strain with increasing defect concentration. A slowly relaxing secondary expansion effect (and/or expansion hysteresis) was also discovered. Possible causes of this behavior, including phase transition/segregation at high vacancy concentration, are discussed.

1. Introduction

Perovskite ceramic materials with high oxygen ionic conductivity have shown promise as electrode materials in solid oxide fuel cells (SOFCs) and as ion-transport membranes for oxygen separation or syngas production.[1−4] Among these, $La_{1-x}Sr_xCoO_{3-\delta}$ (LSC) has been widely studied because of its ability to become reduced reversibly at moderate P_{O_2}, producing high concentrations of oxygen ion vacancies.[5−7] While these vacancies facilitate oxygen ion transport and oxygen surface exchange, they also lead to lattice volume expansion and mechanical stress, a critical factor in determining success or failure in fabricating and using these materials.[7−9]

Previous workers have shown that the LSC family of perovskites expands rapidly at high temperature and constant P_{O_2} because of the reduction of Co (or other B-site transition-metal dopants, such as Fe, Ni, Cr, etc.).[10−13] Subsequent studies of expansion in reduced oxides, including doped and undoped ceria,[8,14,15] doped lanthanum chromite,[8,16] and several browmillerite−perovskite intergrowth oxides,[17−20] have attempted to separate and quantify the chemical

* To whom correspondence should be addressed.
† University of Washington.
‡ Case Western Reserve University.

(1) Singhal, S. C. Application of ionic and electronic conducting ceramics in solid oxide fuel cells. *Proc.—Electrochem. Soc.* **1998**, *97−24*, 125−136.
(2) Steele, B. C. H. Materials for IT-SOFC stacks 35 years R&D: the inevitability of gradualness? *Solid State Ionics* **2000**, *134*, 3−20.
(3) Yamamoto, O. Solid oxide fuel cells: fundamental aspects and prospects. *Electrochim. Acta* **2000**, *45*, 2423−2435.
(4) Steele, B. C. H. Ceramic ion conducting membranes. *Curr. Opin. Solid State Mater. Sci.* **1996**, *1*, 684−691.
(5) Okamoto, H.; Obayashi, H.; Kudo, T. Carbon monoxide gas sensor made of stabilized zirconia. *Solid State Ionics* **1980**, *1*, 319−326.
(6) Mizusaki, J. Nonstoichiometry, diffusion, and electrical properties of perovskite-type oxide electrode materials. *Solid State Ionics* **1992**, *52*, 79−91.
(7) Anderson, H. U. Review of P-Type Doped Perovskite Materials for SOFC and Other Applications. *Solid State Ionics* **1992**, *52*, 33−41.
(8) Atkinson, A.; Ramos, T. Chemically-induced stresses in ceramic oxygen ion-conducting membranes. *Solid State Ionics* **2000**, *129*, 259−269.
(9) Nigel, D. P.; Francis, C. M.; Butt, D.; Doorn, V.; Elias, R. H.; Cutler, Ashton, R. Mixed conducting membranes for syngas production. U.S. Patent 6,492,290, 2002.
(10) Ohno, Y.; Nagata, S.; Sato, H. Properties of Oxides for High-Temperature Solid Electrolyte Fuel-Cell. *Solid State Ionics* **1983**, *9−10*, 1001−1007.
(11) Nagamoto, H.; Mochida, I.; Kagotani, K.; Inoue, H.; Negishi, A. Change of thermal expansion coefficient and electrical conductivity of $LaCo_{1-x}M_xO_3$ (M = Fe, Ni). *J. Mater. Res.* **1993**, *8*, 3158−3162.
(12) Tai, L.-W.; Nasrallah, M. M.; Anderson, H. U.; Sparlin, D. M.; Sehlin, S. R. Structure and electrical properties of $La_{1-x}Sr_xCo_{1-y}Fe_yO_3$. Part 2. The system $La_{1-x}Sr_xCo_{0.2}Fe_{0.8}O_3$. *Solid State Ionics* **1995**, *76*, 273−283.
(13) Tai, L.-W.; Nasrallah, M. M.; Anderson, H. U.; Sparlin, D. M.; Sehlin, S. R. Stucture and electrical properties of $La_{1-x}Sr_xCo_{1-y}Fe_yO_3$. Part 1. The systerm $La_{0.8}Sr_{0.2}Co_{1-y}Fe_yO_3$. *Solid State Ionics* **1995**, *76*, 259−271.
(14) Atkinson, A. *Calculation of the Stress Distribution in Gd-doped Ceria Electrolyte Plates under Operating Conditions*; Department of Materials, Imperial College: London, U.K., pp 707−716.
(15) Atkinson, A. Chemically-induced stresses in gadolinium-doped ceria solid oxide fuel cell electrolytes. *Solid State Ionics* **1997**, *95*, 249−258.
(16) Williford, R. E.; Armstrong, T. R.; Gale, J. D. Chemical and thermal expansion of calcium-doped lanthanum chromite. *J. Solid State Chem.* **2000**, *149*, 320−326.
(17) Armstrong, T. R.; Stevenson, J. W.; Pederson, L. R.; Raney, P. E. Dimensional instability of doped lanthanum chromite. *J. Electrochem. Soc.* **1996**, *143*, 2919−2925.
(18) Armstrong, T. R.; Stevenson, J. W.; McCready, D. E.; Paulik, S. W.; Raney, P. E. The effect of reducing environments on the stability of acceptor substituted yttrium chromite. *Solid State Ionics* **1996**, *92*, 213−223.
(19) Stevenson, J. W.; Armstrong, T. R.; Armstrong, B. L.; Bates, J. L.; Hsieh, G.; et al. *Mixed oxygen ion/electron-conducting ceramics for oxygen separation*; Pacific Northwest National Laboratory: Richland, WA, 1996; pp 117−126.
(20) Prado, F.; Armstrong, T.; Caneiro, A.; Manthiram, A. Structural Stability and oxygen permeation properties of $Sr_{3-x}La_xFe_{2-y}Co_yO_{7-\delta}$ ($0 \le x \le 0.3$ and $0 \le y \le 1.0$). *J. Electrochem. Soc.* **2001**, *148*, J7−J14.

10.1021/cm050905h CCC: $30.25
Published on Web 07/20/2005

expansion (that part of the expansion due to changes in P_{O_2}) from the thermal expansion. To date, however, a complete set of expansion measurements in the LSC family of perovskites (over a wide range of P_{O_2} and T) have not been conducted. The purpose of this study is to separate and quantify thermal and chemical expansion in LSC.

2. Theory

Traditionally, thermal expansion of solid materials is described in terms of a coefficient of thermal expansion (CTE). This description fails to adequately describe mixed conducting oxides, in which the lattice volume is a function of both the temperature and oxidation state (often described in terms of the oxygen-vacancy concentration). As shown by Adler,[21] these strain dependencies can be quantified in terms of the traditionally defined volumetric thermal expansivity (β_T) as well as a volumetric "oxygen-vacancy chemical expansivity" (β_C):

$$\beta_T = \left(\frac{\partial \ln \hat{V}}{\partial T}\right)_{x_v,P} \qquad \beta_C = \left(\frac{\partial \ln \hat{V}}{\partial x_v}\right)_{T,P} \tag{1a,b}$$

where $\hat{V}$ is the specific volume (assumed to be macrohomogeneously isotropic for a polycrystalline sample), T is temperature, P is the total pressure, and x_v is the oxygen-vacancy mole fraction, defined as $x_v = \delta/3$, where δ is the oxygen nonstoichiometry in $ABO_{3-\delta}$. Using these definitions, the total derivative of the uniaxial strain (ϵ) in the absence of pressure or mechanical forces is given by[21]

$$d\epsilon(T,x_v) = \frac{1}{3}\beta_T\, dT + \frac{1}{3}\beta_C\, dx_v \tag{2}$$

Thus, by measurement of the uniaxial strain as a function of T and x_v, it is possible to determine β_T and β_C.

In general, β_T and β_C can themselves be functions of T and x_v. For example, consider a second-order multivariable Taylor expansion of $\epsilon(T,x_v)$ around $T = 25$ °C and $x_v = 0$:

$$\epsilon(T,x_v) = \epsilon(25\ °C,0) + \left(\frac{\partial\epsilon}{\partial T}\right)_{T=25°C,x_v=0}(T-25) + \frac{1}{2}\left(\frac{\partial^2\epsilon}{\partial T^2}\right)_{T=25°C,x_v=0}(T-25)^2 + \left(\frac{\partial\epsilon}{\partial x_v}\right)_{T=25°C,x_v=0}x_v + \frac{1}{2}\left(\frac{\partial^2\epsilon}{\partial x_v^2}\right)_{T=25°C,x_v=0}x_v^2 + \left(\frac{\partial^2\epsilon}{\partial x_v\,\partial T}\right)_{T=25°C,x_v=0}(T-25)x_v \tag{3}$$

Taking the total derivative and matching it to eq 2, one obtains

$$\frac{1}{3}\beta_T(T) = \left(\frac{\partial\epsilon}{\partial T}\right)_{T=25°C,x_v=0} + \left(\frac{\partial^2\epsilon}{\partial T^2}\right)_{T=25°C,x_v=0}(T-25) + \left(\frac{\partial^2\epsilon}{\partial T\,\partial x_v}\right)_{T=25°C,x_v=0}x_v$$

$$\frac{1}{3}\beta_C(x_v) = \left(\frac{\partial\epsilon}{\partial x_v}\right)_{T=25°C,x_v=0} + \left(\frac{\partial^2\epsilon}{\partial x_v^2}\right)_{T=25°C,x_v=0}x_v + \left(\frac{\partial^2\epsilon}{\partial T\,\partial x_v}\right)_{T=25°C,x_v=0}(T-25) \tag{4a,b}$$

Thus, to second order, β_T and β_C will depend linearly on T and x_v, respectively. They will also depend linearly on x_v and T, respectively, through the cross term $[\partial^2\epsilon/(\partial x_v\,\partial T)]_{T=25°C,x_v=0}$, which represents both the temperature dependence of the chemical expansivity and the vacancy concentration dependence of the thermal expansivity. As we will see below, if this term is small, it can be challenging to distinguish experimentally from the other second-order terms $\partial^2\epsilon/\partial x_v^2$ and $\partial^2\epsilon/\partial T^2$.

3. Experimental Section

$La_{1-x}Sr_xCoO_{3-\delta}$ (LSC) powders of compositions $x = 0.2$ (LSC-82), $x = 0.4$ (LSC-64), and $x = 0.7$ (LSC-37) were obtained from Superconductive Components Inc. (SCI; Columbus, OH). These powders were made by the "Sandia Chemical Prep" process, involving mixing and decomposition of inorganic nitrates. Inductively coupled plasma composition analysis provided by SCI indicated that the overall compositions of the materials were accurate to better than 0.5 mol %.

Prior to fabrication of dilatometry samples, we characterized these partially calcined powders using powder X-ray diffraction (XRD). The samples varied in phase purity, with the LSC-82 and -64 powders considerably more phase pure than LSC-37, which showed many peaks that did not index to a perovskite structure.

Samples of LSC-82, -64, and -37 were calcined in air at 1100, 1150, and 1200 °C and examined again with XRD to see if the phase purity improved. Calcined samples of LSC-82 and -64 showed only perovskite peaks within the detection limits of XRD. Following calcinations at 1200 °C, the LSC-37 sample also showed only perovskite peaks. However, repeat experiments approximately 1 year later with LSC-37 on the same powder showed the existence of one small extra peak (~1% of the highest peak amplitude) that could not be indexed to a perovskite. Regrinding and recalcination did not entirely eliminate this peak. An intervening change of venue from Case Western Reserve University to University of Washington makes it difficult to trace this difference because the environment, furnace, and storage history of the powder were not identical at both institutions. It was also impossible to identify the peak because of uncertainty in its location/shape (in the noise of the data) as well as the very large number of possible compounds that could potentially be formed (oxides, sulfides, carbonates, and hydroxides).

Scanning electron microscopy images of all three powders revealed a uniform submicron morphology, and spot analyses with energy-dispersive spectrometry suggested a uniform composition free of other detectable elements. To determine if the slight phase impurity found for more recent samples of LSC-37 has an impact on the expansion, expansion measurements were also conducted on a sample of LSC-37 made by Praxair Surface Technologies (Seattle, WA). The XRD patterns of LSC-37 from Praxair showed a pure perovskite structure.

Dense samples of LSC-82, -64, and -37 were prepared by pressing LSC powders in a square prismatic die, to approximately 45 × 5 × 5 mm. The pressed samples were subsequently isostatically pressed to 150 MPa and sintered to 97−98% of theoretical density at 1200−1250 °C on alumina in air (density measured by the Archimedes method).

(21) Adler, S. B. Chemical expansivity of electrochemical ceramics. *J. Am. Ceram. Soc.* **2001**, *84*, 2117−2119.

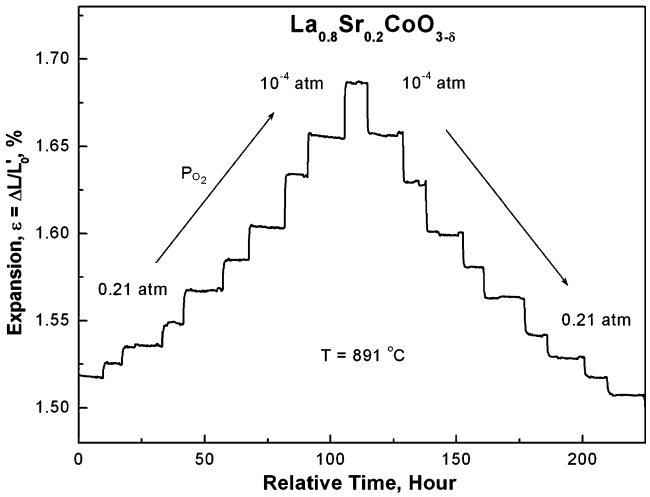

Figure 1. Length variation of dense $La_{0.8}Sr_{0.2}CoO_{3-\delta}$ with time, resulting from P_{O_2} changes between 0.21 and 10^{-4} atm at 891 °C. The specimen length was 43.4 mm at room temperature in air before measurement.

Equilibrium expansion measurements were made using the vacuum-controlled dilatometer system described previously.[21] Typically the sample temperature was ramped slowly (≤2 °C/min) to a particular value, and the sample was allowed to equilibrate for several days in air or in a blended mixture of O_2 in N_2 at 1 atm. Following this, the total pressure was changed in small steps (using a vacuum system) to the desired P_{O_2}, where it was held constant. The main purpose of using small P_{O_2} steps was to avoid the risk of breaking the sample because of the stress generated across the specimen by the expansion. Such stresses occur upon any large, rapid change in P_{O_2} because of the resulting gradient in the oxygen-vacancy mole fraction from inside to outside the sample.[21] After several hours or days of equilibration, the sample expansion was determined, and P_{O_2} was adjusted to the next point. The sample was usually taken down in P_{O_2} to about 10^{-4} atm and then returned in small steps to air (checking for hysteresis, as discussed further in the following section) before moving to the next temperature point. The data presented in this paper constitute a minimum of 40−60 days of measurements per sample. In the case of LSC-37 (which exhibits significant hysteresis), it was necessary to record 25 days of data for a single temperature.

As an example, Figure 1 shows a raw trace of the isothermal expansion of LSC-82 at $T = 891$ °C as P_{O_2} is stepped (via the total pressure) from air to 10^{-4} atm and back. Following each step in P_{O_2}, approximately an hour is required for the expansion to relax to its new equilibrium state. This time scale, which gets longer as the temperature is reduced, represents the rate at which oxygen gas can exchange with the bulk of the sample via adsorption/desorption at the surface and ambipolar diffusion of oxygen through the material. As described below, the equilibrium changes in ϵ vs P_{O_2} at each temperature are used to reconstruct the dependence of the expansion on the temperature and vacancy concentration.

4. Data Analysis

4.1. Modeling of Oxygen Nonstoichiometry. Equations 1−4 describe the uniaxial strain as a function of the temperature and oxygen-vacancy mole fraction, $\epsilon(T,x_v)$. However, our measurements did not directly measure the expansion as a function of x_v but rather $\epsilon(T,P_{O_2})$. To recast our constitutive data in terms of the vacancy concentration, we used a model for the oxygen stoichiometry based on a modification of Lankhorst's Rigid Band Model.[22−26] This model was used to interpolate previously measured oxygen nonstoichiometry properties of $La_{1-x}Sr_xCoO_{3-\delta}$, allowing us to calculate the vacancy concentration x_v under the specific T and P_{O_2} conditions prevailing during our dilatometry measurements.

Lankhorst's original model[22−25] assumes that electrons created during oxygen-vacancy formation are donated to electron states associated with a partially filled metallic band. It is assumed that the density of states at the Fermi level, $g(\epsilon_F)$, is a constant, i.e., a "square" rigid electron band. In our modification of this model,[26] we hypothesize that changes in the stoichiometry are significant enough that band curvature may be important, such that the density of states varies somewhat with electron occupation. We have modeled this effect to first order by allowing $g(\epsilon) = g_0(\epsilon_0) + g_1(\epsilon_0)(\epsilon - \epsilon_0)$, where $g_0(\epsilon_0)$ is the density of states at electron energy ϵ_0, $g_1(\epsilon_0)$ is the first derivative of $g(\epsilon)$, evaluated at electron energy ϵ_0, and ϵ_0 is the Fermi energy when the electron occupation number n_e (as defined by Lankhorst[25]) is given by $n_e = 6x_v - x = 0$. This assumption results in the following implicit expression for $x_v(T,P_{O_2})$:[26]

$$\mu^0_{O_2}(T) + RT\ln P_{O_2} = E_{OX} - TS_{OX} - 2RT\ln\left(\frac{x_v}{1-x_v}\right) - 4\left(\frac{n_e}{g_0(\epsilon_0)} - \frac{n_e^2 g_1(\epsilon_0)}{g_0^3(\epsilon_0)}\right) \quad (5)$$

where E_{OX} and S_{OX} are the energy and entropy terms that are independent of the temperature and oxygen nonstoichiometry and $\mu^0_{O_2}$ is the standard chemical potential of oxygen (a known function of the temperature[22]).

We used the model in eq 5 to fit the experimental nonstoichiometry data of $La_{1-x}Sr_xCoO_{3-\delta}$ ($x = 0.2$, 0.4, and 0.7) as measured by Lankhorst et al.[23] and Mizusaki et al.[27] as a function of the temperature and oxygen partial pressure. For each value of Sr content x, this model was fit simultaneously (using nonlinear least squares) to data covering the available range of $x_v(T,P_{O_2})$. This fit yields the model parameters shown in Table 1. Although we make no comments here about the physical significance of these parameters, we generally found this model to fit the data better than previous models over the range of available data. For example, Figures 2 and 3 show data and accompanying fits for oxygen nonstoichiometry in LSC-91 and LSC-37.

(22) Lankhorst, M. H. R.; Bouwmeester, H. J. M.; Verweij, H. Use of the Rigid Band Formalism to Interpret the Relationship between O Chemical Potential and Electron Concentration in $La_{1-x}Sr_xCoO_{3-\delta}$. *Phys. Rev. Lett.* **1996**, *77*, 2989−2992.
(23) Lankhorst, M. H. R.; Bouwmeester, H. J. M.; Verweij, H. High-temperature coulometric titration of $La_{1-x}Sr_xCoO_{3-\delta}$: Evidence for the effect of electronic band structure on nonstoichiometry behavior. *J. Solid State Chem.* **1997**, *133*, 555−567.
(24) Lankhorst, M. H. R.; Bouwmeester, H. J. M.; Verweij, H. Thermodynamics and transport of ionic and electronic defects in crystalline oxides. *J. Am. Ceram. Soc.* **1997**, *80*, 2175−2198.
(25) Lankhorst, M. H. R.; Bouwmeester, H. J. M.; Verweij, H. Importance of electronic band structure to nonstoichiometric behaviour of $La_{0.8}Sr_{0.2}CoO_{3-\delta}$. *Solid State Ionics* **1997**, *96*, 21−27.
(26) Chen, X.; Adler, S., to be published.
(27) Mizusaki, J.; Mima, Y.; Yamauchi, S.; Fueki, K. Nonstoichiometry of the Perovskite-Type Oxides $La_{1-x}Sr_xCoO_{3-\delta}$. *J. Solid State Chem.* **1989**, *80*, 102−111.

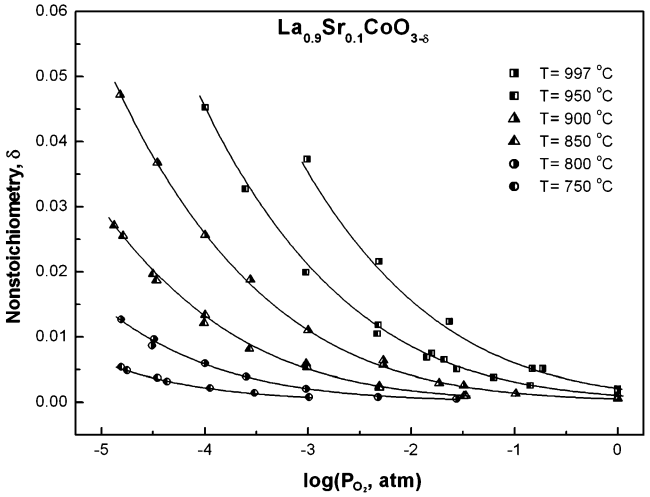

Figure 2. Plot of the oxygen nonstoichiometry δ in $La_{0.9}Sr_{0.1}CoO_{3-\delta}$ as a function of the temperature and oxygen partial pressure. Drawn lines represent the best fits to the modified itinerant electron model. All of the experimental data are taken from Mizusaki et al.[27]

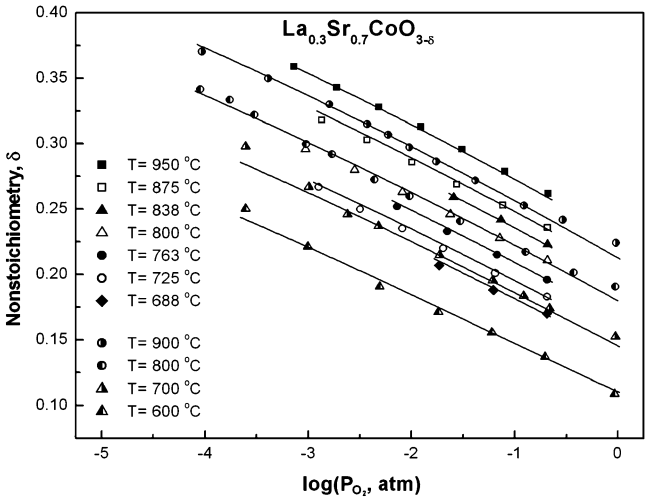

Figure 3. Plot of the oxygen nonstoichiometry δ in $La_{0.3}Sr_{0.7}CoO_{3-\delta}$ as a function of the temperature and oxygen partial pressure. Drawn lines represent the best fits to the modified itinerant electron model. The experimental data represented by half-solid points are taken from Mizusaki et al.[27] and the others from Lankhorst et al.[23]

Table 1. Parameters Obtained from Fitting Published[23,27] Oxygen Nonstoichiometry Data of $La_{1-x}Sr_xCoO_{3-\delta}$ to the Modified Itinerant Electron Model of Equation 5

	$x = 0.1$	$x = 0.2$	$x = 0.4$	$x = 0.7$
E_{OX}, kJ/mol	−387.69	−335.19	−288.57	−246.61
S_{OX}, J/mol·K	55.62	69.10	92.88	137.04
$g_0(\epsilon_F)$, $\times 10^{-5}$ (J/mol)$^{-1}$	3.39	3.06	1.86	1.35
$g_1(\epsilon_F)$, $\times 10^{-10}$ (J/mol)$^{-2}$	114.01	67.89	1.30	−1.83

4.2. Correcting for Expansion Hysteresis. During the chemical expansion experiments described in section 3, we observed hysteresis in the uniaxial strain, which relaxes on a different time scale from changes in the oxidation state. As shown in the raw expansion trace of LSC-82 (Figure 1), the expansion following each change in P_{O_2} undergoes a relatively rapid transient associated with changes in the oxygen content, followed by equilibrium at a relatively stable value. However, small changes in expansion persist throughout the relatively stable period, requiring many hours or days to relax (in some cases in the reverse direction from the initial transient).

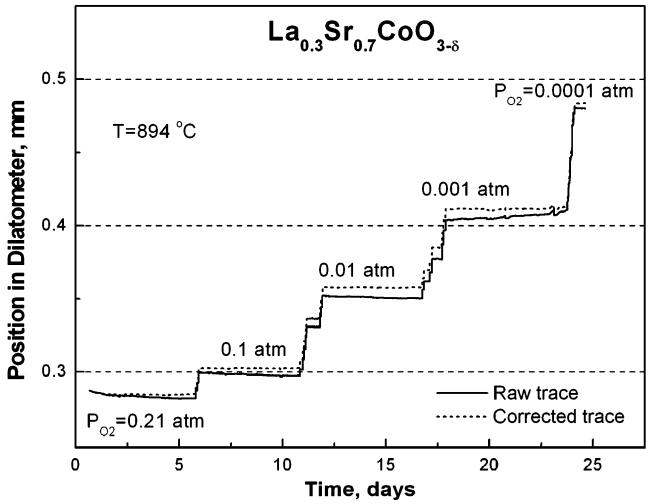

Figure 4. Long-time expansion behavior of LSC-37 at 894 °C and various P_{O_2}'s. The short-dashed line in the figure reflects a corrected trace compared with the raw trace (solid line), according to the correction algorithm described below.

As shown in Figure 4, this behavior was most apparent with LSC-37. Following each P_{O_2} transient, the expansion continues to drift almost linearly with time, reaching no stable state even after many days. At high P_{O_2} ($\geq 10^{-2}$ bar), the drift is negative relative to the initial transient. At low P_{O_2} ($\leq 10^{-3}$ bar), the drift is in the same direction as that of the initial transient. No such phenomenon was observed in "blank" expansion measurements of alumina over the same T and P_{O_2} conditions, confirming that this observation is not an instrumental artifact. These observations were highly repeatable over several measurements and identical for samples made from different starting powders (SCI and Praxair).

Although not shown in Figure 4, the net expansion during one cycle of reducing, and then increasing, P_{O_2} does not trace a reversible path. Even for LSC-82 (Figure 1), the expansion at a given P_{O_2} is different on the path downward in P_{O_2} than on the return path upward in P_{O_2}. For this reason, we report this phenomenon as "hysteresis", although it is possible that these transients would eventually relax to an equilibrium state. Notably, the isothermal expansion of $La_{0.96}MnO_{2.94+\delta}$ appears to demonstrate similar expansion drift upon P_{O_2} step changes.[28]

An obvious concern is that expansion transients could be related to the initial phase purity of LSC-37. If the material were incompletely reacted to a single phase, continued reaction in the dilatometer might produce an added contribution to the expansion. However, if this were the case, we would not expect the direction of expansion drift to depend strongly on P_{O_2} or identical effects to be observed in LSC-37 made by different synthesis routes, having measurable differences in the phase purity. Although the effect may involve phase separation of LSC-37,[29] it appears to be a feature of LSC-37 itself and not an artifact of minor secondary phases unique to the fabrication procedure.

(28) Miyoshi, S.; Hong, J.; Yashiro, K.; Kaimai, A.; Nigara, Y.; Kawamura, K.; Kawada, T.; Mizusaki, J. Lattice expansion upon reduction of perovskite-type $LaMnO_3$ with oxygen-deficit nonstoichiometry. *Solid State Ionics* **2003**, *161*, 209−217.
(29) Chen, X. Y.; Adler, S. B. To be published.

Another question is whether the observed drift in expansion is a secondary source of expansion or simply reflects multiple time scales over which oxygen stoichiometry changes occur. For example, if changes in the oxygen nonstoichiometry required corequisite changes in cation order, part of the stoichiometry changes after a change in P_{O_2} might be limited by cation (rather than anion) diffusion. To test this hypothesis, we have conducted long-term thermogravimetry measurements of LSC-37 following similar step changes in P_{O_2} as in Figure 4.[29] Our results show that the long-term expansion transients are *not* correlated to any change in the oxygen content. Thus, whatever causes this slow drift in expansion does not appear to be related to further changes in the oxidation state.

This leaves two remaining hypotheses that we are currently investigating. The first is that, following each change in the oxidation state, a much slower local rearrangement of cations occurs (not involving further changes in the oxidation state), to obtain a more stable local structural configuration.[30,31] Such microdomains, which may be too small to detect using powder XRD, are frequently observed in highly defective perovskite-type oxides.[32,33] A second (not mutually exclusive) hypothesis is that high oxygen nonstoichiometry in LSC is not stable and results in phase changes or phase segregation.[34,35] We are currently conducting powder XRD studies of LSC-37 powders following quenching from elevated temperatures and various P_{O_2}.[29] To date, we have found that LSC-37 undergoes a phase change or phase segregation at low P_{O_2} (100 ppm), in the same range of P_{O_2} as we observed the expansion hysteresis. However, we are not yet certain whether these phase changes are present at elevated temperature or merely upon quenching.

To proceed with our analysis of the short-term expansion associated directly with oxygen nonstoichiometry, we have attempted to separate the observed expansion into a "primary" chemical expansion associated with short-term transients in oxygen stoichiometry and a "secondary" expansion (of uncertain origin) relaxing over longer time scales. If we assume that the long-term transients are ultimately subject to equilibrium and do not themselves involve a change in the oxygen stoichiometry (as we have confirmed with thermogravimetric analysis), we might modify eq 2 to consider other state variables impacting the lattice volume:

$$\mathrm{d}\ln\epsilon = \frac{1}{3}\beta_T\,\mathrm{d}T + \frac{1}{3}\beta_C\,\mathrm{d}x_v + \sum_i \frac{1}{3}\beta_{\xi i}\,\mathrm{d}\xi_i \qquad (6)$$

where ξ_i represents a relevant state variable (other than x_v) influencing the lattice volume, e.g., an ordering parameter

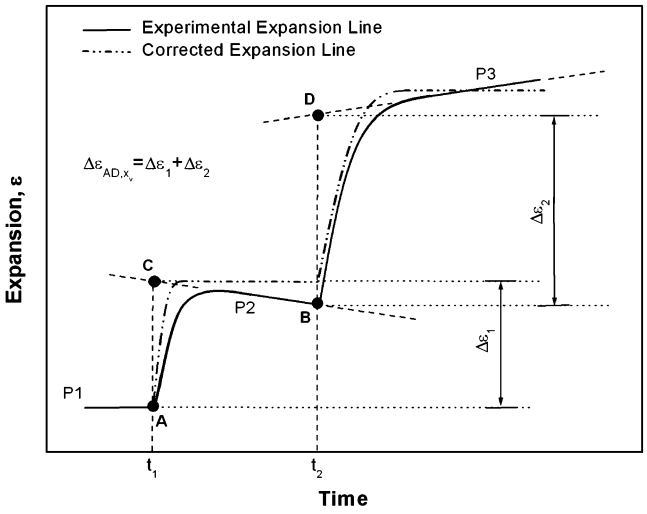

Figure 5. Schematic illustrating the algorithm used to isolate primary chemical expansion associated directly with changes in the oxygen stoichiometry from long-term secondary expansion effects. The solid curve represents the actual total expansion following step changes in P_{O_2} (P1, P2, and P3). The dashed lines represent the linear extrapolation of the long-time secondary expansion transients. The dash-dotted line represents the "corrected" expansion for which the long-term transients have been subtracted. In this schematic, the magnitude of the long-term transient has been exaggerated for clarity.

for cations or a parameter describing phase segregation. Assuming linearity of thermal, chemical, and other expansion effects over small transients, the integral of this equation at constant T leads to

$$\epsilon(T_0,x_v) - \epsilon(T_0,x_{v0}) = \frac{1}{3}\beta_C(x_v - x_{v0}) + \sum_i \Delta\epsilon_{\xi i}(t) \qquad (7)$$

where the last term on the right-hand side represents slowly decaying secondary expansion effects. Assuming that these secondary expansions are slow compared to equilibration of the oxidation state, $(1/3)\beta_C(x_v - x_{v0})$ can be determined by extrapolating the expansion following each step change back toward $t = 0$. Once the equilibrium expansion difference following each instantaneous P_{O_2} step is determined, these can be added segmentwise to reconstruct the net primary equilibrium chemical expansion associated with changes in the oxygen content.

A schematic of our algorithm for this extrapolation is shown in Figure 5. Following each step in P_{O_2}, the sample expansion (solid line) is assumed to reach oxygen diffusional equilibrium relatively quickly compared to the last term in eq 7. Assuming that the secondary expansion is linear with time for short times, the data can be extrapolated backward (to point C) to determine the primary oxygen-vacancy chemical expansion difference between the initial and final states, denoted as $\Delta\epsilon_1$. Subtraction of the long-term trend

(30) Patrakeev, M. V.; Mitberg, E. B.; Lakhtin, A. A.; Kozhevnikov, V. I.; Kharton, V. V.; Avdeev, M. Y.; Marques, F. M. B. Oxygen nonstoichiometry, conductivity and seebeck coefficient of $La_{0.3}Sr_{0.7}Fe_{1-x}Ga_xO_{2.65+\delta}$ perovskites. *J. Solid State Chem.* **2002**, *167*, 203−213.

(31) Kharton, V. V.; et al. Oxygen permeability and ionic conductivity of perovskite-related $La_{0.3}Sr_{0.7}Fe(Ga)O_{3-\delta}$. *J. Electrochem. Soc.* **2002**, *149*, E125−E135.

(32) Hagenmuller, P.; Pouchard, M.; Grenier, J. C. Nonstoichiometry in the perovskite-type oxides: an evolution from the classical Schottky−Wagner model to the recent high Tc superconductors. *Solid State Ionics* **1990**, *43*, 7−18.

(33) Adler, S.; Russek, S.; Reimer, J.; Fendorf, M.; Stacy, A.; Huang, Q.; Santoro, A.; Lynn, J.; Baltisberger, J.; Werner, U. Local Structure and oxide-ion motion in defective perovskites. *Solid State Ionics* **1994**, *68*, 193−211.

(34) Fossdal, A.; Menon, M.; Wærnhus, I.; Wiik, K.; Einarsrud, M.; Gradne, T. Crystal Structure and Thermal Expansion of $La_{1-x}Sr_xFeCo_{3-\delta}$ Materials. *J. Am. Ceram. Soc.* **2004**, *87*, 1952−1958.

(35) Grunbaum, N.; Mogni, L.; Prado, F.; Caneiro, A. Phase equilibrium and electrical conductivity of $SrCo_{0.8}Fe_{0.2}O_{3-\delta}$. *J. Solid State Chem.* **2004**, *177*, 2350−2357.

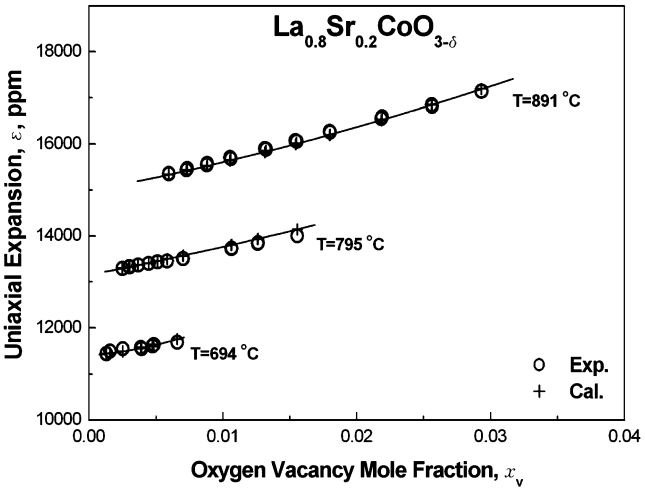

Figure 6. Equilibrium expansion data of LSC-82 ceramics as a function of temperature T and oxygen-vacancy mole fraction x_v. The "+" data represent the best fitting of the experimental data "○" to eq 8.

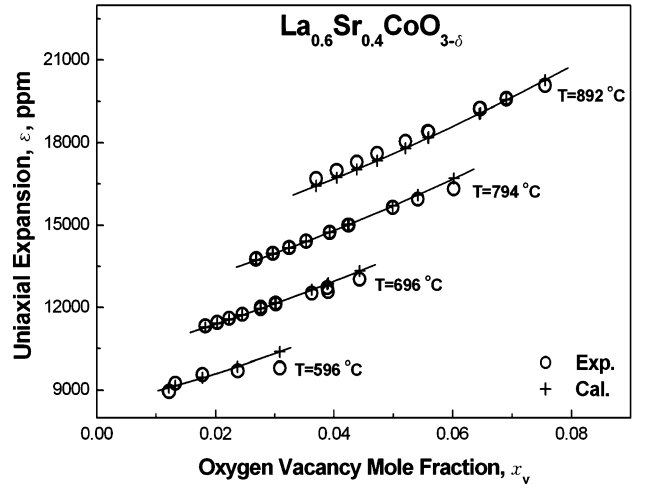

Figure 7. Equilibrium expansion data of LSC-64 ceramics as a function of temperature T and oxygen-vacancy mole fraction x_v. The "+" data represent the best fitting of the experimental data "○" by using eq 8.

from the data results in a "corrected" transient (dash-dotted line). This same basic algorithm is repeated at each P_{O_2} step to determine $\Delta\epsilon_1$, $\Delta\epsilon_2$, $\Delta\epsilon_3$, etc., and then these individual changes in the expansion are added to determine the total oxygen-vacancy chemical expansion independent of secondary effects. "Corrected" data for LSC-37 at 894 °C are shown in Figure 4.

5. Results and Discussion

Figures 6−8 show equilibrium expansion measurements of LSC-82, -64, and -37, respectively, as a function of the temperature and oxygen-vacancy mole fraction, determined using the analysis procedures described above. Again, the oxygen-vacancy mole fractions shown here are based on previous measurements of the oxygen nonstoichiometry,[22] interpolated to the specific T and P_{O_2} conditions of our experiment using a modified itinerant electron model (section 4.1). The data include measurements made on downward and upward steps in P_{O_2} (as shown in Figure 1). In most cases, the points determined from upward and downward transients sit on top of each other, indicating that the primary expansion associated with oxygen nonstoichiometry is reversible once secondary expansion effects have been subtracted. Error bars are estimated to be smaller than the symbols shown.

These data show that the contribution of the oxygen nonstoichiometry to the lattice volume is significant. A 2% change in the oxygen content results in an expansion equivalent to a temperature change of about 100 °C. The thermal and chemical contributions to the expansion appear to be remarkably similar for all of the materials, at all temperatures and values of P_{O_2}. Significant curvature in the chemical expansion is apparent, but it does not appear to contain discontinuities, as might be expected if a first-order phase change were occurring at the lowest P_{O_2}'s.

In principle, one can fit the data in Figures 6−8 to eq 3 in order to obtain best-fit values for the thermal and chemical expansivities. In practice, however, the range of temperatures studied is too narrow to fully resolve the third-order terms $\partial^2\epsilon/\partial x_v^2$, $\partial^2\epsilon/\partial T^2$, and $\partial^2\epsilon/(\partial x_v\,\partial T)$.

To more accurately determine the thermal expansion near 25 °C, we also measured the isobaric expansion at low temperatures (25−300 °C) where the chemical expansion is zero and/or "frozen" at a small value because of slow oxygen diffusion/exchange. These measurements were fit to a parabolic profile [$(\partial\epsilon/\partial T)_{25°C}$ and $(\partial^2\epsilon/\partial T^2)_{25°C}$], and these values were used in subsequent fits of the high-temperature data.

Initial results using this approach showed that the cross term, $\partial^2\epsilon/(\partial x_v\,\partial T)$, is small (usually below 2% of the total chemical expansion) and thus is difficult to resolve with statistical significance. This observation suggests that the thermal and chemical expansions are nearly independent of each other. In this case, the nonlinear expansion (eq 3) can be reduced to

$$\epsilon(T,x_v) - \epsilon(25\ °C,0) = \left(\frac{\partial\epsilon}{\partial T}\right)_{T=25°C,x_v=0}(T-25) + \frac{1}{2}\left(\frac{\partial^2\epsilon}{\partial T^2}\right)_{T=25°C,x_v=0}(T-25)^2 + \left(\frac{\partial\epsilon}{\partial x_v}\right)_{T=25°C,x_v=0}x_v + \frac{1}{2}\left(\frac{\partial^2\epsilon}{\partial x_v^2}\right)_{T=25°C,x_v=0}x_v^2 \quad (8)$$

Table 2 summarizes the results obtained by fitting the data in Figures 6−8 to eq 8 using nonlinear least squares.

To see if our results are consistent with isobaric expansion measurements, we took the values of the thermal and chemical expansions in Table 2 and used them to calculate the isobaric expansion of LSC-37 in air from 30 to 900 °C. Figure 9 compares the result of this calculation to that of the measured isobaric expansion. The calculations agree very precisely at high temperature, where the sample is expected to maintain equilibrium with the ambient T and P_{O_2}. However, at lower temperatures, the expansions agree in slope but are shifted by a constant amount from that predicted by equilibrium.

Estimates of oxygen exchange and diffusion rates (both activated) suggest that they become slower than the sample cooling rate at 300−400 °C, where we see the "knee" in the data. Thus, it appears this discrepancy results from the

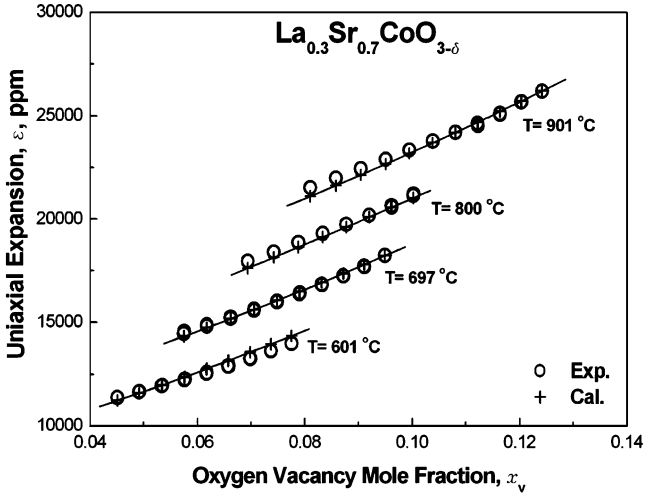

Figure 8. Equilibrium expansion data of LSC-37 ceramics as a function of temperature T and oxygen-vacancy mole fraction x_v. The "+" data represent the best fitting of the experimental data "○" by using eq 8.

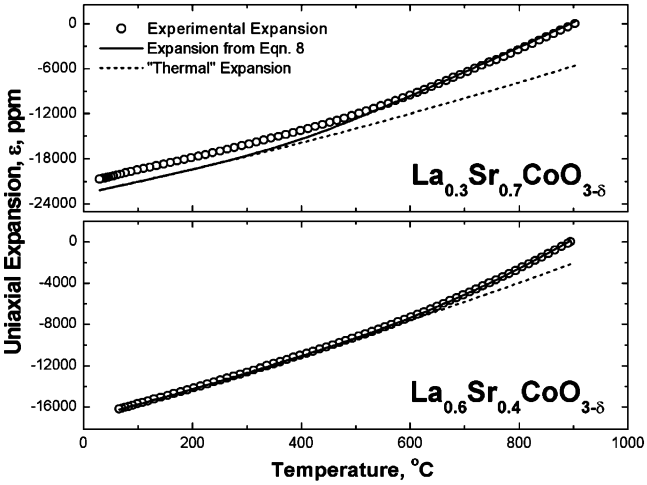

Figure 9. Uniaxial expansion of $La_{0.3}Sr_{0.7}CoO_{3-\delta}$ and $La_{0.6}Sr_{0.4}CoO_{3-\delta}$ in air upon cooling from equilibrium in air at 900 °C. The expansion in this case has been normalized to that prevailing at 900 °C in air. The dotted line shows the calculated contribution of thermal expansion, $\Delta\epsilon_T$, based on the values in Table 2. The solid line adds the contribution of chemical expansion, $\Delta\epsilon_C$, based on the values in Table 2, using eq 8. This comparison illustrates the persistence of nonstoichiometry in samples having a high dopant content upon cooling at a finite rate.

Table 2. Summaries of Thermal and Chemical Expansivities of LSC (x = 0.2, 0.4, and 0.7) by Best Fitting of the Experimental Data in Figures 6−8 to Equation 8

material	$(1/3)\beta_T$ (ppm/°C)	$(1/3)\beta_C$ (ppm/ppm)
LSC-82	$15.92 + 3.06 \times 10^{-3}(T - 25\ °C)$	$0.054 + 1.534x_v$
LSC-64	$14.20 + 4.84 \times 10^{-3}(T - 25\ °C)$	$0.055 + 0.811x_v$
LSC-37	$15.51 + 7.50 \times 10^{-3}(T - 25\ °C)$	$0.062 + 0.561x_v$

oxygen nonstoichiometry "freezing in" as the sample is cooled at a finite rate. Similar behavior has been observed previously for $La_{0.6}Sr_{0.4}Co_{0.2}Fe_{0.8}O_{3-\delta}$.[12,13] Residual nonstoichiometry appears to be higher for materials with higher Sr content, reflecting their higher oxygen nonstoichiometry in the 300−400 °C temperature window.

The results summarized in Table 2 show that the thermal and chemical expansion properties of LSC-82, -64, and -37 are remarkably similar when extrapolated to low vacancy concentration and temperature. To investigate this possibility further, the chemical expansions, $\epsilon_C(x_v)$, of all of the LSC samples were compared by subtracting the thermal expansion

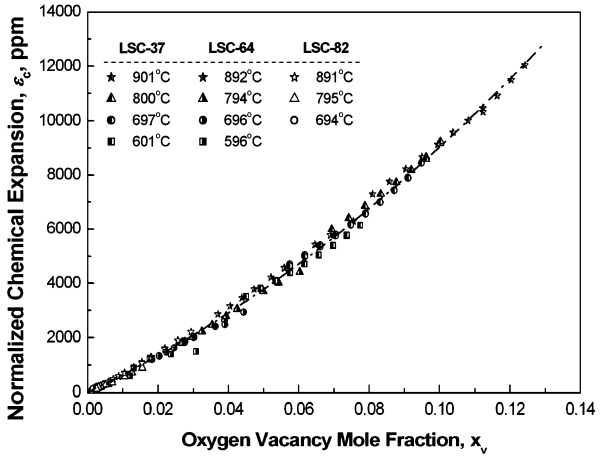

Figure 10. Chemical expansion of LSC ceramics as a function of the oxygen-vacancy mole fraction, normalized as described in the text. The dash-dotted line is given by eq 9.

Table 3. Summaries of Thermal and Chemical Expansivities of LSC (x = 0.2. 0.4, and 0.7) from Different Approaches

material	$(1/3)\beta_T^{avg}$, (ppm/°C)[a]	$(1/3)\beta_C^{avg}$, (ppm/ppm)[b]
LSC-37	17.9	0.139
LSC-64	15.8	0.129
LSC-82	16.5	0.112

[a] Calculated from the expansion data in the low-temperature range (25−450 °C). [b] Calculated from the expansion data in high-temperature range (600−900 °C).

(as calculated using eq 8 based on parameters in Table 2) and normalizing to zero expansion at an extrapolated vacancy concentration of $x_v = 0$. The result of this normalization is shown in Figure 10.

Assuming that the apparent single curve shown in Figure 10 is physically meaningful, a parabolic regression of the data yields a "universal" correlation for chemical expansion in the LSC family of materials:

$$\frac{1}{3}\beta_C(x_v) = 0.061 + 0.584x_v \qquad (9)$$

which is plotted with the data in Figure 10. Care should be taken not to interpret this parabolic correlation too universally, recognizing the restricted range of vacancy concentrations actually measured for each material. Measurements over a wider range of vacancy concentrations in each individual material would be needed to fully validate the universality (and binary dependence) apparent in the data. Nonetheless, the data from all materials at all temperatures are remarkably contiguous, given the range of temperatures and Sr contents represented.

To compare our results to those of other materials in the literature, average uniaxial thermal and chemical expansivities were calculated for relevant temperature and stoichiometry ranges as

$$\frac{1}{3}\beta_T^{avg} = \frac{\int_{T_1}^{T_2}\left(\frac{1}{3}\beta_T(T)\right)dT}{T_2 - T_1} \qquad \frac{1}{3}\beta_C^{avg} = \frac{\int_{x_{v1}}^{x_{v2}}\left(\frac{1}{3}\beta_C(x_v)\right)dx_v}{x_{v2} - x_{v1}} \qquad (10a,b)$$

with the results summarized in Table 3. Over the temperature range 25−450 °C, the average thermal expansivities of LSC-82, -64, and -37 were found to be similar, varying 16−18

Table 4. Experimental and Estimated Chemical Expansivities, (1/3) β_C^{avg}, of Various Perovskite Materials

material	measured[a]	calculated	ref
$LaMnO_{3-\delta}$	0.072[b]	0.078[c] 0.60[d]	28
$La_{0.8}Sr_{0.2}CrO_{3-\delta}$	0.087	0.202	42, 43
$La_{0.76}Sr_{0.24}CrO_{3-\delta}$	0.060		8, 17
$La_{0.7}Sr_{0.3}CrO_{3-\delta}$	0.069		8, 17
$La_{1-x}Sr_xCrO_{3-\delta}$	0.072		8, 44
$La_{0.9}Ca_{0.1}CrO_{3-\delta}$	0.063		42
$La_{0.8}Ca_{0.2}CrO_{3-\delta}$	0.084		42
$La_{0.7}Ca_{0.3}CrO_{3-\delta}$	0.108		8, 17
$La_{1-x}Ca_xCrO_{3-\delta}$	0.075		8, 44
$La_{0.8}Sr_{0.2}CoO_{3-\delta}$	0.112	0.047[c] 0.248[d]	this study
$La_{0.6}Sr_{0.4}CoO_{3-\delta}$	0.129		
$La_{0.3}Sr_{0.7}CoO_{3-\delta}$	0.139		
$La_{0.7}Ca_{0.3}Cr_{0.9}Al_{0.1}O_{3-\delta}$	0.108	0.202[e]	8, 17
$La_{0.7}Ca_{0.3}Cr_{0.9}Ga_{0.1}O_{3-\delta}$	0.075		8, 17
$La_{0.7}Ca_{0.3}Cr_{0.9}Ti_{0.1}O_{3-\delta}$	0.096		8, 17
$La_{0.7}Ca_{0.3}Cr_{0.9}Mn_{0.1}O_{3-\delta}$	0.048		8, 17
$La_{0.7}Ca_{0.3}Cr_{0.9}Co_{0.1}O_{3-\delta}$	0.036		8, 17
$La_{0.7}Ca_{0.3}Cr_{0.9}Fe_{0.1}O_{3-\delta}$	0.060		8, 17
$La_{0.7}Ca_{0.3}Cr_{0.9}Ni_{0.1}O_{3-\delta}$	0.039		8, 17
$La_{0.7}Ca_{0.3}Cr_{0.9}Cu_{0.1}O_{3-\delta}$	0.059		8, 17
$La_{0.7}Ca_{0.3}Cr_{0.9}Zn_{0.1}O_{3-\delta}$	0.066		8, 17
$La_{0.8}Sr_{0.2}Cr_{0.97}V_{0.03}O_{3-\delta}$	0.090		8, 44

[a] Many of the values in this column were estimated based on measurements of $\Delta\epsilon_C/\Delta\delta$ over a finite change in stoichiometry $\Delta\delta$. $(1/3)\beta_C^{avg}$ is comparable to $3\Delta\epsilon_C/\Delta\delta$. [b] Reported value for the oxygen-deficient regime only (low P_{O_2}). [c] Estimated on the basis of low-spin radii if applicable. [d] Estimated on the basis of high-spin ionic radii if applicable. [e] Calculated values of B-site-substituted chromite are close to that of the nonsubstituted chromite due to a large ratio of chromium, regardless of the substituted ionic valence change.

ppm/°C. These values compare favorably with the CTE of other materials of perovskite structure,[16,17−20,30,36−40] including those without large chemical expansivities. The average chemical expansivity, calculated in the temperature range 600−900 °C, was found to be between 0.11 and 0.14 ppm/ppm. This increase in $(1/3)\beta_C^{avg}$ with the Sr content simply reflects the fact that the chemical expansion is nonlinear (as illustrated in Figure 10) and that the average vacancy concentration is higher for materials with higher Sr content.

Table 4 compares the results summarized in Table 3 to the oxygen-vacancy chemical expansion of selected perovskites reported in the literature.[8,12,18,21,28,30,34,42−44] These values suggest that all perovskites have similar values of chemical expansion, with $(1/3)\beta_C^{avg}$ falling somewhere in the 0.06−0.15 range, depending on the dopant and dopant concentration. In the case of LSC, we saw that most of this variation arises from the nonlinearity observed in Figures 6−9 rather than an explicit dependence on the dopant concentration. This raises the possibility that the variations seen in the average β_C among materials in Table 4 may also be due, in part, to variations in the vacancy concentration. Further investigation of this possibility via studies of the type presented in this paper would be needed to address this question.

The reason that the chemical expansion appears to accelerate with increasing vacancy concentration remains somewhat unclear. Numerous workers have attempted to correlate the isothermal chemical expansion with changes in the average ionic radii of cations.[8,17,28,34,42−44] With this view, charge disproportionation of the B-site cation (resulting from the introduction of oxygen vacancies) is assumed to occur, and the weighted average radius is calculated based on the ionic radii corresponding to the individual disproportionated oxidation states.[28] Relating the predicted lattice volume changes to the definitions in eqs 1 and 2, we would expect

$$\frac{1}{3}\beta_C = \frac{1}{3}\left(\frac{\partial \ln \hat{V}}{\partial x_v}\right)_{T,P} \cong \frac{\ln(\hat{V}_1/\hat{V}_0)}{3\Delta x_v} = \frac{\ln\{[(a_0+\Delta a)/a_0]^3\}}{\Delta\delta} \cong \frac{3\Delta a}{\Delta\delta \cdot a_0} = \frac{6\Delta \bar{r}_B}{\Delta\delta \cdot a_0} \quad (11)$$

where a_0 is the pseudocubic lattice parameter (~3.9 Å at zero oxygen nonstoichiometry) and $\bar{r}_B$ is the average radius of the B-site ion. The change in the average ionic radius ($\Delta\bar{r}_B$) is related to the change in the oxidation state ($\Delta\delta$) by considering the weighted average of the radii of the trivalent and tetravalent B ions:

$$\bar{r}_B = \frac{[B_B^{\bullet}]r_{B_B^{\bullet}} + [B_B^{\times}]r_{B_B^{\times}}}{[B]} \quad (12)$$

where the concentrations of trivalent and tetravalent B-site ions are derived from the site balance and charge neutrality conditions:

$$[Sr'_{La}] = 2[V_O^{\bullet\bullet}] + [B_B^{\bullet}]$$

$$[B_B^{\bullet}] + [B_B^{\times}] = [B] \quad (13a,b)$$

where $[Sr'_{La}] = x$ and $[V_O^{\bullet\bullet}] = \delta$. Combining eqs 11−13, the relationship between the chemical expansivity of perovskite oxides and the variation of the average radius of the B-site ion is given by

$$\frac{1}{3}\beta_C = \frac{12(r_{B_B^{\times}} - r_{B_B^{\bullet}})}{a_0} \quad (14)$$

(36) Qiu, L.; Ichikawa, T.; Hirano, A.; Imanishi, N.; Takeda, Y. $Ln_{1-x}Sr_xCo_{1-y}FeyO_{3-\delta}$ (Ln = Pr, Nd, Gd; x = 0.2, 0.3) for the electrodes of solid oxide fuel cells. *Solid State Ionics* **2003**, *158*, 55−65.

(37) Ullmann, H.; Trofimenko, N.; Tietz, F.; Stover, D.; Khanlou, A. A. Correlation between thermal expansion and oxide ion transport in mixed conducting perovskite-type oxides for SOF cathodes. *Solid State Ionics* **2000**, *138*, 79−90.

(38) Kharton, V. V.; Yaremchenko, A. A.; Patrakeev, M. V.; Naumovich, E. N.; Marques, F. M. B. Thermal and chemical induced expansion of $LaSr(Fe, Ga)O_{3-\delta}$ ceramics. *J. Eur. Ceram. Soc.* **2003**, *23*, 1417−1426.

(39) Stevenson, J. W.; Hasinska, K.; Canfield, N. L.; Armstrong, T. R. Influence of cobalt and iron additions on the electrical and thermal properties of $(La, Sr)(Ga, Mg)O_{3-\delta}$. *J. Electrochem. Soc.* **2000**, *147* (9), 3213−3218.

(40) Hayashi, H.; Suzuki, M.; Inaba, H. Thermal expansion of Sr- and Mg-doped $LaGaO_3$. *Solid State Ionics* **2000**, *128*, 131−139.

(41) Shannon, R. D. Revised effective ionic radii and systematic studies of interatomic distances in halides and chalcogenides. *Acta Crystallogr.* **1976**, *A32*, 751−767.

(42) Boroomand, F.; Wessel, E.; Bausinger, H.; Hilpert, K. Correlation between defect chemistry and expansion during reduction of doped $LaCrO_3$ interconnects for SOFCs. *Solid State Ionics* **2000**, *129*, 251−258.

(43) Zuev, A.; Singheiser, L.; Hilpert, K. Defect structure and isothermal expansion of A-site and B-site substituted lanthanum chromites. *Solid State Ionics* **2002**, *147*, 1−11.

Table 5. Shannon Effective Ionic Radii, in Å, for Selected Ions[a,41]

Cr^{4+}	Cr^{3+}	Fe^{4+}	Fe^{3+}(HS)	Co^{4+}(HS)	Co^{3+}(HS)	Co^{3+}(LS)	V^{4+}	V^{3+}	Mn^{4+}	Mn^{3+}(HS)	Mn^{2+}(HS)	Mn^{2+}(LS)
0.55	0.615	0.585	0.645	0.53	0.61	0.545	0.58	0.64	0.53	0.645	0.83	0.67

[a] All of the radii were selected in 6-fold coordination. LS, HS: low-spin and high-spin configurations, respectively.

Equation 14 predicts a linear dependence of the chemical expansion on the vacancy concentration, with a constant value of β_C. When the Shannon effective ionic radii[41] are applied in octahedral coordination (Table 5), the linear chemical expansivities of various perovskite oxides can be estimated from eq 14. The estimated chemical expansivities are compared with the experimental values in Table 4.

As can be seen in Table 4, the estimated chemical expansivities based on this approach are generally 2−5 times higher than that measured experimentally, assuming that the spin configuration of the B-site cation does not also change upon a change in the oxidation state.[28]

In the case of LSC, the spin state of Co in LSC has been a matter of considerable study and debate.[45−51] Low and intermediate temperature magnetic measurements seem to suggest that, with increasing temperature or Sr doping, the spin configuration of Co changes gradually from low spin to intermediate spin (or high spin). It is therefore possible that some portion of the nonlinearity seen in Figure 10 is associated with this spin-state transition. However, to explain such small values of the chemical expansion in LSC based solely on this argument, one must assume Co^{4+} is low spin, while Co^{3+} is high spin, which does not seem likely given our current understanding of the electronic structure in these materials.[45]

These considerations suggest that the ionic radius and oxidation state are insufficient to fully explain the chemical expansion; other factors must be involved, such as local lattice distortions and/or preferred coordination. To further illustrate this point, Figure 11 shows a replotting of the chemical expansion data for LSC (shown in Figure 10) as a function of the Co oxidation state, reported in terms of the electron occupation number,[25] $n_e = 6x_v - x$. When Figures 10 and 11 are compared, it would appear that the chemical

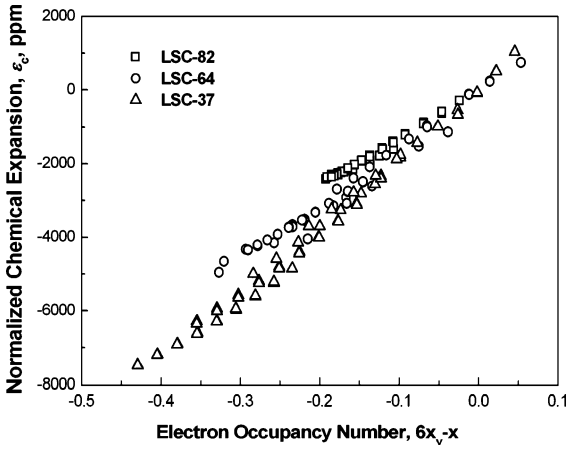

Figure 11. Chemical expansion of LSC as a function of the Co oxidation state, as described in the text.

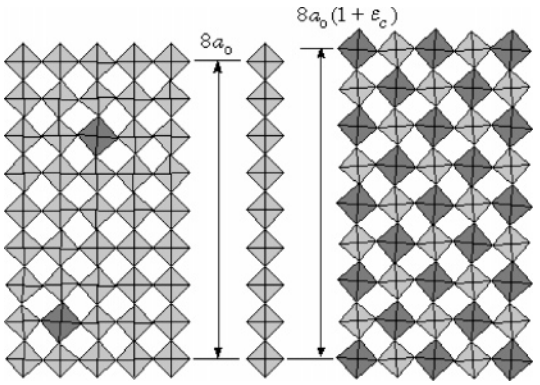

Figure 12. Qualitative explanation of why expansion may be nonlinear with the vacancy concentration. MO_6 octahedra of initial dimension a_0 (light gray) experience an average increase in the bond length (dark gray) near an oxygen vacancy. At low concentration, the net expansion is much less than the average bond length because the other bonds surrounding the enlarged octahedron must shorten for it to fit within the surrounding lattice. At higher concentrations, cooperative ordering processes may occur that lessen the lattice strain.

expansion in LSC is more strongly tied to the vacancy concentration than to the oxidation state.

One possible explanation for this apparent dependence on the vacancy concentration is the lattice strain associated with doping in a three-dimensional (3-D) lattice. Equation 14 essentially assumes a one-dimensional lattice, where substitution of an alioradiant cation translates directly into a change in the average lattice parameter. However, as illustrated in Figure 12, in a 3-D lattice any change in the average bond length in the vicinity of a vacancy cannot occur without distortion of the surrounding lattice. The strain associated with this distortion will generally act to counterbalance the longer bond lengths in the vicinity of the vacancy. As the vacancy concentration increases, however, one expects that the alioradiant cations will begin to interact spatially, reducing this strain energy and allowing increasing volume expansion for a given number of substitutions.

On the basis of a mean-field argument, we might expect such an effect to result in an increasing binary term at higher

(44) Larsen, P. H.; Hendriksen, P. V.; Mogensen, M. Dimensional stability and defect chemistry of doped lanthanum chromites. *J. Therm. Anal.* **1997**, *49*, 1263−1275.
(45) Señarís-Rodríguez, M. A.; Goodenough, J. B. Magnetic and transport properties of the system $La_{1-x}Sr_xCoO_{3-\delta}$ ($0 < x \leq 0.50$). *J. Solid State Chem.* **1995**, *11*, 323−336.
(46) Yamaguchi, S.; Okimoto, Y.; Ishibashi, K.; Tokura, Y. Magnetooptical Kerr effects in perovskite-type transition-metal oxides: $La_{1-x}Sr_xMnO_3$ and $La_{1-x}Sr_xCoO_3$. *Phys. Rev. B* **1998**, *58*, 6862−6870.
(47) Caciuffo, R.; Rinaldi, D.; Barucca, G.; Mira, J.; Rivas, J.; Señarís-Rodríguez, M. A.; Radaeli, P. G.; Fiorani, D.; Goodenough, J. B. Structural details and magnetic order of $La_{1-x}Sr_xCoO_{3-\delta}$ ($0 < x \leq 0.30$). *Phys. Rev. B* **1999**, *59*, 1068−1078.
(48) Ravindran, P.; Korzhavyi, P. A.; Fjellvag, H. H.; Kjekshus, A. Electronic structure, phase stability, and magnetic properties of $La_{1-x}Sr_xCoO_3$ from first-principles full-potential calculations. *Phys. Rev. B* **1999**, *60*, 16423−16434.
(49) Baio, G.; Barucca, G.; Caciuffo, R.; Rinaldi, D.; Mira, J.; Rivas, J.; Señarís-Rodríguez, M. A.; Fiorani, D. Phase separation, thermal history and magnetic behaviour of Sr doped $LaCoO_3$. *J. Phys. Condens. Matter* **2000**, *12*, 9761−9770.
(50) Ravindran, P.; Fjellvag, H. H.; Kjekshus, A.; Blaha, P.; Schwarz, K.; Luitz, J. Itinerant metamagnetism and possible spin transition in $LaCoO_3$ by temperature/hole doping. *J. Appl. Phys.* **2002**, *91*, 291−303.
(51) Wu, J.; Leighton, C. Glassy ferromagnetism and magnetic phase separation in $La_{1-x}Sr_xCoO_3$. *Phys. Rev. B* **2003**, *67*, Art. No. 174408.

vacancy concentrations, as proposed, for example, by Lankhorst in the context of vacancy enthalpy.[22] This would be consistent with the apparent parabolic dependence seen in Figure 10. On the other hand, if the material experiences a phase instability at high vacancy concentration (as we suspect it does from the expansion hysteresis), it is perhaps surprising that the interaction would appear only binary over such a wide range of vacancy concentrations. This interpretation would require that any phases formed by ordering or segregation of vacancies would all have similar dependences of the lattice volume on the vacancy concentration, such that the volume-averaged expansion of the polycrystalline material would exhibit a uniform trend, even when local variations in the vacancy concentration prevailed. Such a situation might be plausible, for example, if local vacancy interactions generally mimicked ordering processes at higher concentrations, such as the formation of ordered microdomains[33] or the formation of reduced-symmetry perovskite-like phases.[52]

6. Conclusions

The equilibrium thermal expansivity, β_T, and oxygen-vacancy chemical expansivity, β_C, of $La_{1-x}Sr_xCoO_{3-\delta}$ ($x = 0.2$, 0.4, and 0.7) have been measured using controlled-atmosphere dilatometry. The averaged values of $(1/3)\beta_T$ in the temperature range 25−450 °C were found to fall in a similar range for all materials, varying between 16 and 18 ppm/°C, with a moderate temperature dependence. The chemical expansivity of all three materials was also found to be similar, following a consistent nonlinear trend over the range of data studied, with $(1/3)\beta_C(x_v) = 0.061 + 0.58x_v$. One possible explanation for this nonlinear dependence is the relaxation of the lattice strain as more oxygen vacancies are introduced into the lattice.

Secondary expansion effects and/or expansion hysteresis were also observed in the dilatometric measurements. This hysteresis appears as a linear drift in the expansion over several days following a P_{O_2} transient. Experimental artifacts, or slow changes in the oxygen stoichiometry, have been eliminated as explanations. We are currently investigating the possibility that LSC experiences phase instability at a high vacancy concentration, even when the temperature is very high (900 °C). Interestingly, this phase instability has little effect on the oxygen-vacancy chemical expansivity β_C, possibly because the volume-average properties of the sample remain similar even when vacancies cluster or segregate.

Acknowledgment. This study was supported by the National Science Foundation under DMR Grants 0222001 and 0222002. The authors are sincerely grateful to Ryan P. Reed and Arne Biemens (UW) and Lu'ay Zeatoun and Bob Lescovec (CWRU) for assistance in building the controlled-atmosphere dilatometer used in these measurements.

CM050905H

(52) Adler, S. B.; Reimer, J. A.; Baltisberger, J.; Werner, U. Chemical Structure and dynamics in $Ba_2In_2O_5$. *J. Am. Chem. Soc.* **1994**, *116*, 675−681.